Dalton Transactions

RSC Publishing

PAPER

View Article Online
View Journal | View Issue

Cite this: *Dalton Trans.*, 2013, **42**, 10559

Iridium(III) complexes with enhanced film amorphism as guests for efficient orange solution-processed single-layer PhOLEDs with low efficiency roll-off†

Jun Dai,‡[a] Kaifeng Zhou,‡[b] Ming Li,[a] Huiqin Sun,[c] Yunqing Chen,[a] Shijian Su,*[b] Xuemei Pu,[a] Yan Huang*[a] and Zhiyun Lu*[a,d]

By introducing a phenyl substituent into the *meta*-site of the phenyl segment of the 2-phenylbenzothiazole ligand, two novel orange iridium(III) complexes, namely, **(3Phbt)$_2$Ir(acac)** and **(3OMePhbt)$_2$Ir(acac)**, have been synthesized. Compared with their parent compound **(bt)$_2$Ir(acac)**, both of them possess much enhanced thermostability and film amorphism, making them suitable candidates as guests for high performance solution-processed phosphorescent organic light-emitting diodes (PhOLEDs). However, **(4Phbt)$_2$Ir(acac)** bearing *para*-phenyl possesses worse processability relative to **(bt)$_2$Ir(acac)** due to spontaneous crystallization stemming from the intense intermolecular interactions. Single-layer solution-processed PhOLEDs with **(3Phbt)$_2$Ir(acac)** and **(3OMePhbt)$_2$Ir(acac)** as guests show peak current efficiency of 17.2 cd A^{-1} and 15.2 cd A^{-1}, and maximum brightness of 28 270 cd m^{-2} and 27 900 cd m^{-2}, respectively. Both are greatly improved compared to the devices employing **(bt)$_2$Ir(acac)** (10.2 cd A^{-1} and 14 350 cd m^{-2}) and **(4Phbt)$_2$Ir(acac)** (5.0 cd A^{-1} and 13 790 cd m^{-2}) as phosphors. Moreover, quite low efficiency roll-off is acquired in these devices at high luminance. The much improved electroluminescence performances of these objective complexes could be mainly attributed to the presence of a rigid phenyl on the appropriate substitution site of the cyclometallate ligand, which leads to improved thermostability with compatible alleviated intermolecular interactions, and consequently enhanced film amorphism.

Received 28th March 2013,
Accepted 9th May 2013

DOI: 10.1039/c3dt50834j

www.rsc.org/dalton

Introduction

Phosphorescent organic light-emitting diodes (PhOLEDs) employing iridium(III) complexes as emitter have attracted much interest because of their capability for harvesting both singlet and triplet excitons efficiently,[1] and based on enormous research efforts, many high performance PhOLEDs with various emission colors have been demonstrated successfully.[2] However, to facilitate charge-injection and transport within the device, most of the high performance PhOLEDs have multilayered device structures fabricated *via* sequential vacuum deposition of small molecules with different functions, which is time-consuming and costly.[3] In contrast to thermal evaporation method, the solution-processing technique is more promising with respect to the cut down of fabrication cost as well as the realization of large-area display and lighting. In particular, as the intermiscibility of the interfaces between the upper and lower layers is considered to be a big problem in multilayered solution-processed devices, it would be more advantageous if both carrier-transporting materials (*i.e.* electron and hole transporting ones) and emissive guests could be integrated into only one active layer.[4] Yet despite many breakthroughs achieved in solution-processed PhOLEDs with iridium complexes as emissive materials,[5] high performance single-layered ones are relatively few.[6]

As the cyclometallate ligands (C^N ligands) of the phosphorescent iridium complexes generally possess conjugated planar geometries, in condensed state, they often show strong tendency toward developing small crystallites due to the

[a]*College of Chemistry, Sichuan University, Chengdu, 610064, P. R. China. E-mail: luzhiyun@scu.edu.cn, huangyan@scu.edu.cn; Fax: +86-28-85410059*
[b]*State Key Laboratory of Luminescent Materials and Devices (South China University of Technology) and Institute of Polymer Optoelectronic Materials and Devices, South China University of Technology, Guangzhou, 510640, P. R. China. E-mail: mssjsu@scut.edu.cn; Fax: +86-20-87110606*
[c]*Analytical and Testing Center, Sichuan University, Chengdu, 610064, P. R. China*
[d]*Key Laboratory of Green Chemistry and Technology, Ministry of Education, Sichuan University, Chengdu, 610064, P. R. China*

†Electronic supplementary information (ESI) available: Crystallographic data of **(bt)$_2$Ir(acac)**, **(4Phbt)$_2$Ir(acac)** and **(3Phbt)$_2$Ir(acac)** (CCDC 857633, 857631 and 818631, respectively). The crystal structures, crystal data and structure refinement, TGA thermograms and POM images, calculated optimized geometry structures and parameters of the corresponding compounds, cyclic voltammograms, ^{1}H NMR, ^{13}C NMR and HR-ESI-MS spectra of the objective compounds are given in Fig. S1–S16 and Tables S1–S3. For ESI and crystallographic data in CIF or other electronic format see DOI: 10.1039/c3dt50834j

‡These authors contribute equally to this article.

relatively strong intermolecular π–π interactions, which would lead to adverse self-quenching, triplet–triplet annihilation (TTA), and formation of interstices as well, hence resulting in deteriorated device performances.[7] Consequently, to be solution-processable by itself with good amorphism stability and less inclination towards crystallization should be an important merit for emissive iridium complexes,[8] since good morphology could be maintained during the post-annealing process or under prolonged electric stress and high working temperatures.[9] To suppress the intermolecular interactions between π-conjugated segments of phosphors, the widely adopted strategies include constructing chelates with hyperbranched dendritic/starbursted structures,[6c,f,10] and nonplanar tetrahedral/spiro structures,[11] which need elaborate and tedious synthetic procedures.[12] In contrast, incorporating bulky substituents with the complex ligands should be a simple yet effective method to obstruct intermolecular π–π interaction.[13] Compared to aliphatic sterically congested substituents, the introduction of aromatic ones would bring multiple torsion barriers that break the molecular planarity, which is favourable to the suppression of molecular π-packing.[7c,14] Accordingly, decorating molecules with aromatic rather than aliphatic substituents should result in compounds with good amorphism,[15] thermostability,[16] and carrier-mobility.[17] Nevertheless, although in the case of electrofluorescent materials, phenyl-modification has been demonstrated to be an effective method to improve both film amorphism and thermal stability of the compounds,[14b,18] correlative studies between aryl substituents and thermal/morphological stability of electrophosphorescent complexes are mainly focused on fluorenyl,[5d,19] carbazyl[20] and diphenylamino[6a,c,13a] groups, while very few investigations have been launched into whether the simplest phenyl-modification would result in iridium chelates with improved amorphism.[21]

Recently, in searching for electrophosphorescent iridium complexes with alleviated self-quenching characteristics, we developed a series of iridium complexes bearing a *para*-phenyl substituent on the phenyl moiety of 2-phenylbenzothiazole (**bt**) ligand, *i.e.* **(4Phbt)$_2$Ir(acac)** (molecular structure shown in Scheme 1) and its derivatives.[22] However, although all these complexes exhibit good PL quantum yields (PLQYs) in solution, **(4Phbt)$_2$Ir(acac)** is found to show even worse film-formation capability than **(bt)$_2$Ir(acac)**, and could not be spin-coated from solution to give a high-quality neat film due to its spontaneous crystallization (evidenced by the intense crystallite signals in its X-ray diffractogram, see Fig. 1b). It should be pointed out that opposite to Li's report[8] that they could not get high-quality neat film of **(bt)$_2$Ir(acac)** *via* spin-coating, a continuous and homogeneous film of **(bt)$_2$Ir(acac)** is easily obtained according to our experimental results (see Fig. 1a). As these observations suggest that the phenyl-modification on C^N ligand impairs rather than enhances the film amorphism of the chelates, which seems to contradict with the literature reports,[21] to elucidate the reason, X-ray crystallographic analysis has been carried out on **(4Phbt)$_2$Ir(acac)** and **(bt)$_2$Ir(acac)**. As shown in Fig. 2, although the biphenyl segment of **(4Phbt)$_2$Ir(acac)** reveals a desirable contorted geometry, there exists quite close intermolecular contact between the phenyl substituents, whereas no significant π–π stacking interaction could be found in **(bt)$_2$Ir(acac)**. Therefore, the spontaneous crystallization characteristics of **(4Phbt)$_2$Ir(acac)** might be ascribed to the intense interactions between the phenyl substituents locating at the relatively spacious *para*-position, hence moving the phenyls to the more congested *meta*-site might be beneficial for the alleviation of π–π interaction between the phenyl substituents. Herein, we report two orange-emitting iridium complexes bearing *meta*-phenyl substituents on **(bt)$_2$Ir(acac)**, namely, bis[2-(biphenyl-3-yl)benzothiazole-*N*,$C^{2'}$]-

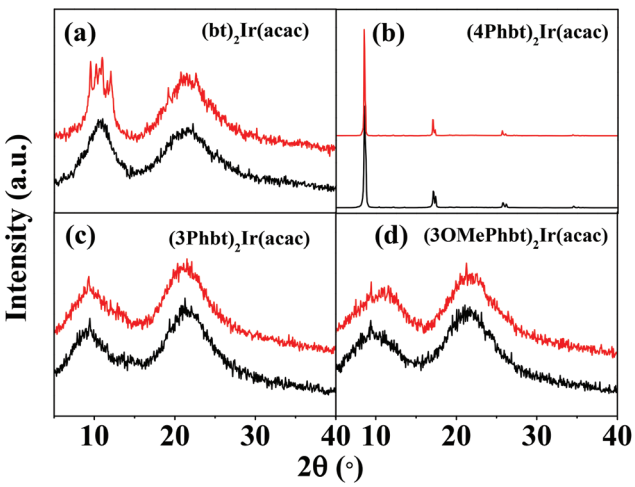

Fig. 1 XRD patterns for the neat films of (a) **(bt)$_2$Ir(acac)**, (b) **(4Phbt)$_2$Ir(acac)**, (c) **(3Phbt)$_2$Ir(acac)**, (d) **(3OMePhbt)$_2$Ir(acac)** (black line: pristine film, red line: after being annealed at 140 °C for 30 min in vacuum).

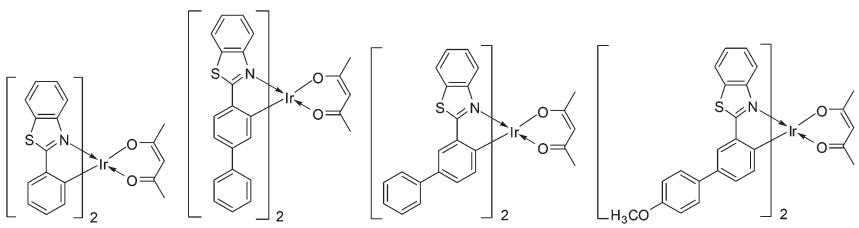

Scheme 1 Molecular structures of the complexes.

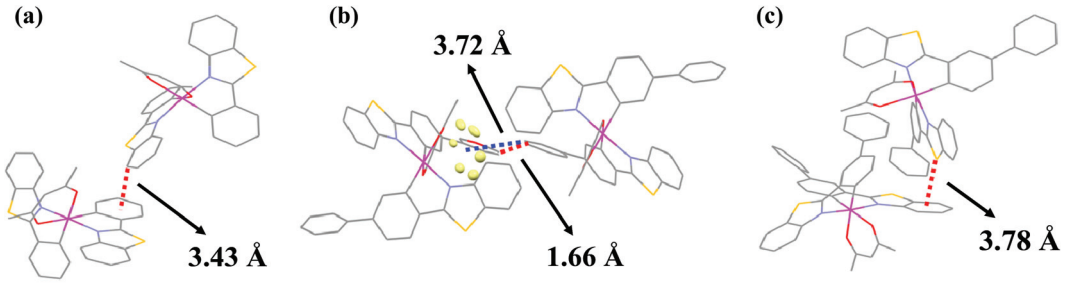

Fig. 2 Crystal packing diagrams of **(bt)$_2$Ir(acac)** (a), **(4Phbt)$_2$Ir(acac)** (b) and **(3Phbt)$_2$Ir(acac)** (c).

iridium(III)(acetylacetonate) [**(3Phbt)$_2$Ir(acac)**] and bis[2-(4′-methoxybiphenyl-3-yl)benzothiazole-*N*,$C^{2'}$]iridium(III)(acetylacetonate) [**(3OMePhbt)$_2$Ir(acac)**]. Both of them possess better morphological and thermal stability in film state relative to **(bt)$_2$Ir(acac)**, and much enhanced amorphism than **(4Phbt)$_2$Ir(acac)** and **(bt)$_2$Ir(acac)**. Single-layer solution-processed PhOLEDs using them as guests show much improved electroluminescence (EL) performance, *i.e.*, higher luminance and efficiency, and lower efficiency roll-off, indicating that the substitution position for phenyl groups on the C^N ligand is an essential factor that determines the amorphism of iridium complexes.

Experimental section

General information and materials

All the reagents involved in the synthetic procedure were commercially available and used without further purification unless otherwise stated. All the solvents were of analytical grade and freshly distilled prior to use. Anhydrous *N*-methylpyrrolidinone and 2-ethoxyethanol were prepared by freshly distilling over calcium hydride and diphosphorous pentoxide, respectively. ^{1}H NMR and ^{13}C NMR spectra were measured on a Bruker AVANCE-400 spectrometer in $CDCl_3$ or DMSO-d_6 using TMS as internal standard. The purity of key intermediates and target molecules were determined by HPLC (Agilent 1100). High resolution MS spectra were obtained from a Q-TOF Priemier ESI mass spectrometer (Micromass, Manchester, UK). Thermogravimetric analysis (TGA) and differential scanning calorimetry (DSC) were performed on TGA Q500 and DSC Q100 instruments under nitrogen atmosphere at a heating rate of 10 °C min^{-1}, respectively. Optical analyses were made through polarized optical microscopy (POM) with ECLIPSE LV 100 POL polarizing microscope equipped with a HCS 621V hot stage and a digital camera, and the heating rate was 1 °C min^{-1}. The PL emission spectra of both solution and thin-film samples were recorded on a PerkinElmer LS55 fluorescence spectrophotometer at 298 K. The UV-vis absorption spectra were measured on a Hitachi U-4100 UV-vis-NIR scanning spectrophotometer. The absolute PL quantum yields (PLQYs) of the doped films were determined with an integrating sphere (IS80 from Labsphere) together with a digital photometer (S370 from UDT) under ambient conditions, under excitation at 340 nm. The morphology of the doped thin films was analyzed through atomic force microscopy (AFM) in tapping mode under ambient conditions using a MFP 3D Asylum Research instrument. The concentration of solution samples for PL measurements was 10^{-5} mol L^{-1} (in CH_2Cl_2). Most of the film samples were obtained by spin-coating from corresponding chlorobenzene solution with concentration of 20 mg mL^{-1} at a speed of 2000 rpm for 40 s on quartz substrates. X-ray diffraction (XRD) data of the film samples were obtained using the Philips DX-100 sealed-tube X-ray generator (Cu target; I = 0.2 nm) with power of 40 kV and 25 mA, and the relatively thick film samples were spin-coated from corresponding chloroform solution with concentration of 40 mg mL^{-1} at a speed of 600 rpm for 40 s on quartz substrates. Cyclic voltammetry (CV) measurement was carried out in argon-purged 5×10^{-4} mol L^{-1} anhydrous CH_2Cl_2 solution with 0.1 mol L^{-1} tetrabutylammonium perchlorate as supporting electrolyte at a scanning rate of 100 mV s^{-1} using a PARSTAT 2273 electrochemical workstation. The CV system was constructed using a platinum plate, a Ag/$AgNO_3$ (0.1 mol L^{-1} in acetonitrile) electrode and a platinum wire as the working electrode, quasi-reference electrode and counter electrode, respectively. Each measurement was calibrated with a ferrocene/ferrocenium (Fc/Fc^+) redox couple as internal standard.

X-Ray diffraction study

The crystallographic data for **(bt)$_2$Ir(acac)**, **(3Phbt)$_2$Ir(acac)** and **(4Phbt)$_2$Ir(acac)** reported here have been deposited in the Cambridge Structural Database (CCDC 857633, 857631 and 818631). Single crystal X-ray diffraction data of the complexes were obtained on an Xcalibur E X-ray single crystal diffractometer equipped with graphite monochromator Mo-Kα (λ = 0.71073 Å) radiation. The data collection was executed using CrysAlisPro program.[23] The structures were determined using direct method and successive Fourier difference syntheses (SHELXS-97) and refined using full-matrix least squares procedure on F^2 with anisotropic thermal parameters for all non-hydrogen atoms (SHELXL-97). Packing analysis of the crystal cells was carried out using Mercury program.[24]

Computational method

For complexes **(bt)$_2$Ir(acac)**, **(3Phbt)$_2$Ir(acac)** and **(3OMePhbt)$_2$Ir(acac)**, B3LYP[25] geometry optimization were performed using LANL2DZ[26] basis set for Ir and 6-31G(d) basis sets for C, H, S,

N and O atoms. All the geometries were confirmed as stationary structures by the presence of only real frequencies at the same level of theory. Orbital energies were calculated within the framework of the IEF-PCM Model[27] in CH_2Cl_2 media based on the optimized geometries. All calculations were carried out with Gaussian09 software.[28]

OLED fabrication and measurements

Indium-tin oxide (ITO) glass substrate with sheet resistance of 15–20 Ω per square was thoroughly cleaned in an ultrasonic bath with acetone, isopropyl alcohol, detergent, de-ionized water and isopropyl alcohol in sequence, and finally treated in UV–ozone chamber under oxygen plasma for 20 min. Then a 40 nm layer of poly(3,4-ethylenedioxythiophene):poly(styrenesulfonate) (PEDOT:PSS) (CLEVIOS P VP AI 4083) was spin-coated from water solution onto the ITO substrates under ambient conditions with a speed of 2000 rpm for 40 s, followed by baking at 200 °C for 10 min in nitrogen. Poly(*N*-vinylcarbazole) (PVK), 1,3-bis[(4-*tert*-butylphenyl)-1,3,4-oxadiazolyl]-phenylene (OXD-7) and the Ir(III) complexes were dissolved in chlorobenzene with concentration of 20 mg mL^{-1}, and the weight percentage of them in the active layer is 67 wt%, 27 wt%, and 6 wt%, respectively. Then the emissive layer was spin-casted from this solution at 2000 rpm for 40 s in a glove box (VAC Co.) with N_2 circulation (with <1 ppm oxygen and water), followed by thermo-annealing treatment at 140 °C for 30 min in N_2 atmosphere. The thickness of the active layer was measured to be ~70 nm. The single-layer devices were completed by thermoevaporation of metal cathode consisting of 3 nm Ba covered by 120 nm Al in vacuum under a pressure of 3×10^{-4} Pa. The thickness of the polymer layer was determined by measuring the thickness of the reference film prepared under very similar conditions with profilometry (Dektak 150 surface profiler). The EL spectra and CIE coordination characteristics were recorded on a PR-705 Spectroscan spectrometer. The current density–voltage–luminance (*J–V–L*) characteristics of PhOLEDs were measured with a calibrated silicon photodiode driven by Keithley 236 source.

Synthesis

The objective molecules and detailed synthetic routes for intermediates are shown in Schemes 1 and 2, respectively. 3-Bromobenzoic acid, 4-bromoanisole and phenylboronic acid were purchased from Aldrich Co. Intermediates methyl 3-bromobenzoate[29] and 4-methoxyphenylboronic acid[30] were synthesized according to the literature reports.

General procedure for the synthesis of 1[31]

Methyl 3-bromobenzoate (0.21 g, 1.0 mmol), appropriate boronic acid (1.1 eq.), $K_3PO_4 \cdot 3H_2O$ (0.55 g, 3 eq.) and $Pd(PPh_3)_4$ (5.8 mg, 0.005 eq.) were added in 20 mL of argon degassed dioxane in a flask. After stirring at 90 °C for 7 h under argon, the mixture was cooled to room temperature and poured into 100 mL water followed by extraction with ethyl acetate (3 × 20 mL). The organic layer was washed with water and brine, then dried over anhydrous Na_2SO_4. After the removal of solvent, the crude product residue was purified by column chromatograph over silica using petroleum ether–dichloromethane (10/1) as eluent to yield the pure product as pale yellow oil. Yield: **1a**: 84.9%; **1b**: 90.4%.

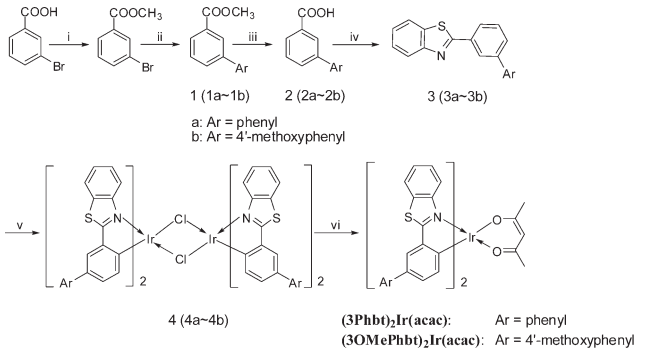

Scheme 2 The synthetic routes of the objective iridium(III) complexes. Reagents and reaction conditions for the synthetic procedures: (i) CH_3OH, concentrated H_2SO_4; (ii) dioxane, arylboronic acid, $Pd(PPh_3)_4$, $K_3PO_4 \cdot 3H_2O$, 90 °C; (iii) (a) CH_3OH, NaOH, reflux, (b) concentrated HCl; (iv) (a) $SOCl_2$, reflux, (b) *o*-aminothiophenol, NMP, 100 °C; (v) $IrCl_3 \cdot 3H_2O$, 2-ethoxyethanol–H_2O = 3/1, 110 °C; (vi) acetylacetone, 2-ethoxyethanol, Na_2CO_3, 110 °C.

General procedure for the synthesis of 2[31]

A solution of **1** (10.0 mmol), 50% aqueous NaOH (2.0 equiv.) and methanol (25 mL) was refluxed for 2 h, then methanol was removed. The residue was dissolved in 25 mL water and acidified with concentrated hydrochloric acid to pH = 1.0. The white precipitate was collected, dried, and used directly for the next step. Yield: **2a**: 89.4%; **2b**: 72.1%.

General procedure for the synthesis of cyclometallate ligands 3[32]

10 mmol of carboxylic acid **2** was refluxed with 20 mL thionyl chloride for 1.5 h, then excessive thionyl chloride was removed under reduced pressure. The corresponding acid chloride was dissolved in 20 mL *N*-methylpyrrolidinone (NMP), then added slowly to a solution of 10 mmol of *o*-aminothiophenol in 20 mL NMP under inert atmosphere at 0 °C. After that, the solution was heated to 100 °C and stirred for 3 h. After cooling, the mixture was poured into water followed by neutralization with 7 mol L^{-1} aqueous ammonia to pH = 8–9. The precipitate was collected and purified by column chromatograph over silica using petroleum ether–dichloromethane (3/1) as eluent to yield the pure product as a white solid.

2-(Biphenyl-3-yl)benzo[*d*]thiazole (3a). White solid. Yield: 60.2%; m.p.: 117 °C; ^{1}H NMR ($CDCl_3$, 400 MHz), δ (ppm): 8.34 (s, 1H), 8.13 (d, J = 8.0 Hz, 1H), 8.09 (d, J = 8.0 Hz, 1H), 7.94 (d, J = 8.0 Hz, 1H), 7.74 (d, J = 8.0 Hz, 1H), 7.71 (d, J = 7.6 Hz, 2H), 7.60 (t, J = 7.6 Hz, 1H), 7.54–7.48 (m, 3H), 7.43–7.39 (m, 2H).

2-(4′-Methoxybiphenyl-3-yl)benzo[*d*]thiazole (3b). White solid. Yield: 70.4%; m.p.: 123 °C; ^{1}H NMR ($CDCl_3$, 400 MHz), δ (ppm): 8.29 (s, 1H), 8.11 (d, J = 8.4 Hz, 1H), 8.03 (d, J = 7.6 Hz, 1H), 7.94 (d, J = 8.0 Hz, 1H), 7.69 (d, J = 7.6 Hz, 1H), 7.64 (d, J = 8.4 Hz, 2H), 7.56–7.49 (m, 2H), 7.42 (t, J = 7.6 Hz, 1H), 7.03 (d, J = 8.4 Hz, 2H), 3.88 (s, 3H).

General procedure for the synthesis of target iridium(III) complexes

Dichloro-bridged iridium(III) complexes were prepared by refluxing $IrCl_3 \cdot 3H_2O$ (1 mmol) with the ligands **3** (2.4 mmol) in a mixture of 2-ethoxyethanol and water (v/v = 3/1) under argon for 24 h.[33] The precipitate was filtered and washed with water, methanol and hexane in sequence, and dried *in vacuo* to afford intermediate **4**. Then it (0.1 mmol) was mixed with acetylacetone (0.3 mmol), anhydrous sodium carbonate (1 mmol) and 10 mL 2-ethoxyethanol, and the reaction mixture was refluxed under argon for 12 h. After being cooled down, the precipitates were collected and purified by flash chromatography over silica using petroleum ether and dichloromethane as mobile phase, followed by recrystallization more than three times to render satisfied purity, then dried for 24 h at 100 °C under vacuum of 1.5 kPa.

Bis[2-(biphenyl-3-yl)benzothiazole-*N*,$C^{2'}$]iridium(III)(acetylacetonate) (3Phbt)$_2$Ir(acac). Red solid. Recrystallized from benzene/methanol. Yield: 46.2%; purity: 99.56%. ^{1}H NMR ($CDCl_3$, 400 MHz), δ (ppm): 8.15–8.13 (m, 2H), 7.95–7.93 (m, 2H), 7.86 (s, 2H), 7.52 (d, J = 8.0 Hz, 4H), 7.48–7.45 (m, 4H), 7.38 (t, J = 8.0 Hz, 4H), 7.27–7.24 (m, 2H), 6.92 (d, J = 8.0 Hz, 2H), 6.54 (d, J = 8.0 Hz, 2H), 5.17 (s, 1H), 1.80 (s, 6H). ^{13}C NMR ($CDCl_3$, 100 MHz), δ (ppm): 185.84, 180.28, 150.86, 147.51, 142.49, 141.27, 135.36, 134.44, 131.37, 129.23, 128.64, 127.43, 126.55, 126.47, 125.26, 124.24, 122.37, 120.21, 101.74, 28.43. ESI-MS: m/z 887.1312 (M + Na^+); Calcd. for M_w + Na^+: 887.1354.

Bis[2-(4′-methoxybiphenyl-3-yl)benzothiazole-*N*,$C^{2'}$]iridium(III)(acetylacetonate) (3OMePhbt)$_2$Ir(acac). Red solid. Recrystallized from dichloromethane/methanol. Yield: 40.2%; purity: 99.61%. ^{1}H NMR (DMSO-d_6, 400 MHz), δ (ppm): 8.31 (d, J = 8.0 Hz, 2H), 7.99 (d, J = 8.0 Hz, 2H), 7.94 (s, 2H), 7.61–7.56 (m, 4H), 7.55 (d, J = 8.0 Hz, 4H), 6.97 (d, J = 8.0 Hz, 4H), 6.91 (d, J = 8.0 Hz, 2H), 6.31 (d, J = 8.0 Hz, 2H), 5.23 (s, 1H), 3.76 (s, 6H), 1.74 (s, 6H). ^{13}C NMR ($CDCl_3$, 100 MHz), δ (ppm): 185.81, 180.33, 150.50, 150.90, 146.63, 142.41, 135.28, 134.12, 133.94, 131.38, 129.00, 127.56, 127.40, 125.21, 123.88, 122.35, 120.21, 114.07, 101.72, 55.27, 28.44. ESI-MS: m/z 947.1509 (M + Na^+); Calcd. for M_w + Na^+: 947.1565.

Results and discussion

Synthesis

The syntheses of complexes **(bt)$_2$Ir(acac)** and **(4Phbt)$_2$Ir(acac)** have been reported by us previously,[22a] and the two objective complexes are prepared following a similar procedure with the products in satisfactory yields and purity. Their molecular structures have been characterized by ^{1}H NMR, ^{13}C NMR, and HR-ESI-MS spectrometry, and **(3Phbt)$_2$Ir(acac)** is further characterized by single crystal X-ray diffraction method.

Thermal, XRD and X-ray crystallographic characterizations

The thermal properties of the four complexes have been investigated by thermogravimetric analysis (TGA) and differential scanning calorimetry (DSC) (TGA diagrams shown in ESI,† data summarized in Table 2). All these complexes exhibit high decomposition temperatures (T_d) of >300 °C (at 5 wt% loss). The phenylation on **bt** ligand is demonstrated to be favourable for the enhancement of the chelates' thermostability, since **(4Phbt)$_2$Ir(acac)**, **(3Phbt)$_2$Ir(acac)** and **(3OMePhbt)$_2$Ir(acac)** all possess higher T_ds (8–29 °C) relative to **(bt)$_2$Ir(acac)**. According to DSC measurements, all these complexes show decomposition prior to melting transition. As shown in Fig. 3, no distinct T_g could be identified for **(4Phbt)$_2$Ir(acac)**; only an inconspicuous phase transition at 141 °C could be observed for **(bt)$_2$Ir(acac)**; while **(3Phbt)$_2$Ir(acac)** and **(3OMePhbt)$_2$Ir(acac)** are found to form stable amorphous glasses with well-defined T_g values of 209 °C and 185 °C, respectively. Further investigations on phase transition characteristics of these compounds have been conducted through polarizing optical microscopy (shown in ESI†). Consistent with the DSC measurements, the polycrystalline **(4Phbt)$_2$Ir(acac)** sample obtained *via* recrystallization is found to show good morphological stability in its crystallite state, since no evident phase transition could be observed in a wide temperature region of 10–260 °C. Nevertheless, although the T_g of **(bt)$_2$Ir(acac)** is not quite distinct in DSC thermogram, an anisotropic–isotropic transition is observable at a rather low temperature of 135 °C. As far as **(3Phbt)$_2$Ir(acac)** and **(3OMePhbt)$_2$Ir(acac)** are concerned, obvious anisotropic–isotropic transitions are distinguishable when they are heated to 210 °C and 182 °C, respectively, which might be assigned to the formation of amorphous glass. Therefore, the phenylation on either *meta*- or *para*-sites of phenyl moiety of **bt** ligand is favourable for the morphological stability of the complexes, yet the *meta*-substitution would result in better amorphism with much enhanced T_g, which is highly desirable for applications in OLEDs.[34] The slightly lowered T_g of **(3OMePhbt)$_2$Ir(acac)** should be ascribed to the presence of alkoxy substituents.[35]

The X-ray diffractograms (XRD) of the four complexes spin-coated film samples are illustrated in Fig. 1. **(4Phbt)$_2$Ir(acac)** shows very poor film-forming capability, since sharp and intense diffraction signals are discernable in its XRD diffractogram. However, for the other three compounds, smooth and

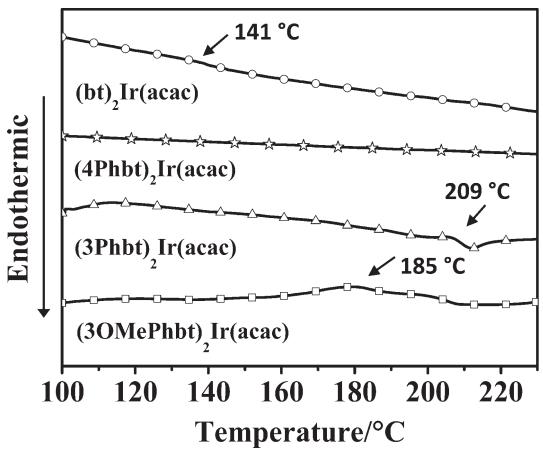

Fig. 3 DSC traces of the four complexes.

continuous amorphous films could be obtained. To evaluate the morphological stability of the phosphors, thermo-annealing treatment has been conducted on the films at 140 °C for 30 min in vacuum. As depicted in Fig. 1, newly emerged diffraction signals could be found in **(bt)$_2$Ir(acac)** after annealing, indicative of the thermoinduced amorphous–crystalline phase transition; however, for **(3Phbt)$_2$Ir(acac)** and **(3OMePhbt)$_2$Ir(acac)**, their XRD traces of pre- and post-thermotreated films are very similar. Therefore, the alteration of the phenyl substituent from *para*- to *meta*-site of **bt** ligand should be quite effective for the enhancement of film amorphism.

To elucidate the correlation between phenylation position and morphological property, single crystal X-ray diffraction analysis has been conducted on **(bt)$_2$Ir(acac)**, **(3Phbt)$_2$Ir(acac)** and **(4Phbt)$_2$Ir(acac)**. The crystallographic refinement parameters, selected bond distances as well as bond angles of the three compounds are summarized in Tables S1 and S2,† and their crystal structures are shown in Fig. S4 (ESI†). The crystal packing diagrams of the three complexes are depicted in Fig. 2. The biphenyl moieties of both **(4Phbt)$_2$Ir(acac)** and **(3Phbt)$_2$Ir(acac)** are found to show distorted geometries, with relative large dihedral angles of ~30° or ~50°. In **(4Phbt)$_2$Ir(acac)**, there should exist relatively intense intermolecular interaction, since the shortest face-to-face ring contact and/or edge-to-face ring contact between the two phenyl substituents are ~1.66 Å and ~3.72 Å, respectively (Fig. 2b). In sharp contrast, no intense intermolecular interaction is discernable in **(3Phbt)$_2$Ir(acac)**, since the shortest edge-to-face distance between π-systems is calculated to be as large as 3.78 Å. Although the single crystal sample of **(3OMePhbt)$_2$Ir(acac)** has not been obtained, similar conformation can be safely assumed in view of its structural similarity to **(3Phbt)$_2$Ir(acac)**. Therefore the better amorphism of **(3Phbt)$_2$Ir(acac)** and **(3OMePhbt)$_2$Ir(acac)** relative to **(4Phbt)$_2$Ir(acac)** may be attributed to their noncoplanar geometries with compatible alleviated intermolecular interactions.

Photophysical properties

The optical absorption and photoluminescence (PL) spectra of the four complexes in 10^{-5} mol L^{-1} CH_2Cl_2 solution are displayed in Fig. S6 (in ESI†) and Fig. 4, respectively, and data are summarized in Table 1. Analogous to many Ir(III) complexes,[36] two absorption bands arising from spin-allowed ligand-based $^1(\pi–\pi^*)$ transitions (below 380 nm) and metal-to-ligand charge-transfer transitions (^{1}MLCT and ^{3}MLCT) (380–550 nm) are distinguishable in all these chelates. With respect to the MLCT transition bands, the λ_{ab} of **(3Phbt)$_2$Ir(acac)** is slightly bathochromic-shifted relative to **(bt)$_2$Ir(acac)**, indicative of its enlarged conjugation systems; and **(3OMePhbt)$_2$Ir(acac)** bearing electron-donating methoxy groups displays a more red-shifted absorption band than **(3Phbt)$_2$Ir(acac)**. Nevertheless, **(4Phbt)$_2$Ir(acac)** shows the most bathochromic-shifted λ_{ab} in both the two major bands, suggesting that the *para*-phenylation is more effective with regard to the expansion of conjugation length.

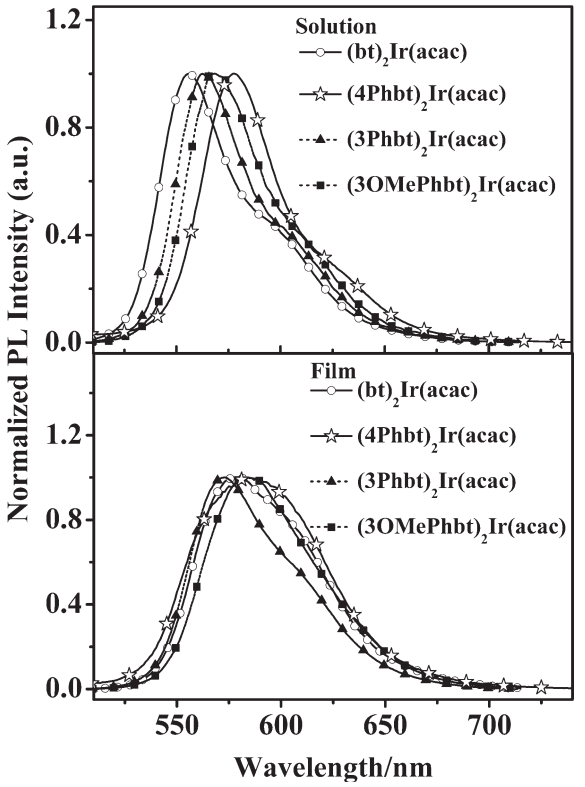

Fig. 4 Normalized PL spectra of the iridium complexes in 10^{-5} mol L^{-1} CH_2Cl_2 solution and solid films at 298 K (under excitation at 400 nm).

In accordance with the UV-vis absorption characteristics, upon irradiation at 400 nm at room temperature, the λ_{PLmax} of these phenyl-modified complexes in dilute solution are red-shifted relative to **(bt)$_2$Ir(acac)**, whose λ_{PLmax} is 555 nm. **(3Phbt)$_2$Ir(acac)** and **(3OMePhbt)$_2$Ir(acac)** have their λ_{PLmax} located at 561 nm and 568 nm, respectively, while **(4Phbt)$_2$Ir(acac)** possesses a λ_{PLmax} of 578 nm. In neat films, all these complexes show broader and more red-shifted PL emission spectra than those acquired from solution (Fig. 4). It is noteworthy that although in solution the PL emission of **(3Phbt)$_2$Ir(acac)** is more red-shifted relative to **(bt)$_2$Ir(acac)**, its λ_{PLmax} is shorter than that of **(bt)$_2$Ir(acac)** (573 nm *vs.* 579 nm) in neat films. In fact, for **(bt)$_2$Ir(acac)** and **(4Phbt)$_2$Ir(acac)**, the difference between λ_{PLmax} in film and solution is as large as 24 nm and 20 nm, respectively, suggesting there exists severe aggregation in condensed states of these two compounds,[37] while those for the two objective compounds are only 12–14 nm, indicative of the more alleviated intermolecular interactions in the two objective complexes.

As the PL emission spectrum of PVK has an effective overlap with the MLCT transition absorption bands of these chelates (shown in Fig. S6†), PVK might be a suitable host for these complexes. Consequently, PL emission spectra and quantum yields (QYs) of the complex/PVK films with different blending ratios have been measured (spectra shown in Fig. S7,† data summarized in Table 1). The presence of residual emission of PVK at even 6 wt% doping level, which

Table 1 Photophysical data of the complexes studied here and the PLQYs of complex/PVK blended thin films at different doping levels

Compound	λ_{ab}[a] (nm) (log ε)	λ_{PLmax}[b] (nm)	λ_{PLmax}[c] (nm)	PLQY[d] (%)				PLQY[e] (%)
				1 wt%	2 wt%	6 wt%	10 wt%	6 wt%
(bt)$_2$Ir(acac)	313(4.4), 326(4.5), 356(3.9), 400(3.9), 440(3.7), 480(3.6)	555	579	39.7	38.8	30.6	16.4	16.6
(4Phbt)$_2$Ir(acac)	311(4.7), 331(4.8), 341(4.8), 417(4.0), 464(3.9), 501(3.8)	578	598	25.3	25.1	19.0	11.8	15.2
(3Phbt)$_2$Ir(acac)	304(4.8), 406(4.8), 456(3.8), 486(3.7)	561	573	38.8	39.1	30.4	16.0	24.8
(3OMePhbt)$_2$Ir(acac)	305(4.9), 408(3.8), 462(3.7), 494(3.7)	568	582	33.3	34.8	27.5	15.2	22.9

[a] UV-vis absorbance is determined in 10^{-5} mol L^{-1} CH_2Cl_2 solution at 298 K. [b] PL emission spectra are acquired in 10^{-5} mol L^{-1} CH_2Cl_2 solution at 298 K, under excitation of 400 nm. [c] Thin films are spin-coated from 20 mg mL^{-1} chlorobenzene solution, PL spectra are obtained under irradiation of 400 nm. [d] Absolute PLQYs of the doped films are measured under ambient conditions (under irradiation of 340 nm). [e] Absolute PLQYs of the post-annealed (140 °C for 30 min in vacuum) 6 wt% doped films are measured under ambient conditions (under irradiation of 340 nm).

could not be suppressed by addition of OXD-7 (27 wt%) (Fig. S8†) suggests incomplete energy transfer between PVK and these guests. As far as PLQY is concerned, the PLQYs of **(3Phbt)$_2$Ir(acac)** and **(bt)$_2$Ir(acac)**-based films are comparable at identical doping levels, while **(4Phbt)$_2$Ir(acac)**-based films exhibit much lower PLQYs compared with the other three complex-based ones. Despite the fact that peak PLQYs are obtained at a doping level of 1 wt% for all these four guests, fairly good efficiencies still could be achieved at blending level of 6 wt%. Yet when the concentration is increased to 10 wt%, the PLQYs drop drastically, which should be ascribed to the self-quenching of the iridium phosphors.

Electrochemical data

The electrochemical properties of the four chelates have been investigated by cyclic voltammetry (CV) in degassed 5×10^{-4} mol L^{-1} CH_2Cl_2 solution with Fc/Fc^+ redox couple as internal standard, and the voltammograms are shown in the ESI,† data are summarized in Table 2. During the anodic scan, each of the chelates shows a quasireversible one-electron oxidation wave which is generally assigned to the Ir^{IV}/Ir^{III} oxidation.[38] The E_{ox}^{onset} are determined to be 0.55 V, 0.52 V, 0.51 V, and 0.42 V relative to Fc/Fc^+ for **(bt)$_2$Ir(acac)**, **(4Phbt)$_2$Ir(acac)**, **(3Phbt)$_2$Ir(acac)** and **(3OMePhbt)$_2$Ir(acac)** in sequence, hence by comparison with the Fc/Fc^+ redox couple whose energy level is 4.80 eV in vacuum, their HOMO energy levels are roughly calculated to be −5.35 eV, −5.32 eV, −5.31 eV, and −5.22 eV, respectively. As no reduction wave could be detected due to the limited range available in CH_2Cl_2, their LUMO energy levels of −3.19 to −3.07 eV are deduced from the HOMO energies and corresponding optical bandgaps.[38] Compared to **(bt)$_2$Ir(acac)**, the *meta*-phenylation on **bt** ligand leads to slightly elevated HOMO energy levels, and the addition of *para*-methoxy groups results in further lowered oxidative potential; whereas these substituents have little effect on the LUMOs of the chelates. It should be pointed out that these observations differ significantly from those of *para*-phenyl modified **(4Phbt)$_2$Ir(acac)**, whose LUMO level is found to be lowered while HOMO level is unchanged.[22a]

Theoretical calculation

To gain insights into the substituent effects of phenyl on photophysical and electrochemical properties of the complexes, DFT calculations were performed using Gaussian09 software for these complexes, and the calculation results of **(4Phbt)$_2$Ir(acac)** could be found in our previous work.[22a] The optimized structures for **(bt)$_2$Ir(acac)**, **(3Phbt)$_2$Ir(acac)** and **(3OMePhbt)$_2$Ir(acac)** along with the numbering of important atoms, main geometrical parameters calculated, and some experimental data derived from X-ray crystallography can be found in the ESI (shown in Fig. S5 and Table S3†). The close similarity between calculated and experimental values confirms the reliability of our computation results. Consistent with the experimental observations for **(3Phbt)$_2$Ir(acac)**, the

Table 2 Electrochemical and thermal data of the iridium complexes

Compound	E_{ox}^{onset}[a,b] (V)	E_g[c] (eV)	HOMO[d] (eV)	LUMO[e] (eV)	HOMO[f] (eV)	LUMO[f] (eV)	T_g[g] (°C)	T_d[h] (°C)
(bt)$_2$Ir(acac)	0.55	2.25	−5.35	−3.10	−5.28	−1.80	141	326
(4Phbt)$_2$Ir(acac)	0.52	2.13	−5.32	−3.19	−5.29	−1.91	—	355
(3Phbt)$_2$Ir(acac)	0.51	2.21	−5.31	−3.10	−5.20	−1.85	209	348
(3OMePhbt)$_2$Ir(acac)	0.42	2.15	−5.22	−3.07	−5.07	−1.82	185	334

[a] Oxidation potential values are measured in 5×10^{-4} mol L^{-1} CH_2Cl_2 solutions. [b] Potential values are reported *versus* Fc/Fc^+. [c] E_g are estimated from the onset wavelength of the optical absorption bands. [d] HOMO energies are deduced from the equation HOMO = 4.8 + E_{ox}^{onset}. [e] LUMO energies are obtained from the equation LUMO = HOMO + E_g. [f] Obtained from B3LYP calculations within the framework of the IEF-PCM model in CH_2Cl_2 media. [g] Obtained from DSC measurements. [h] Temperatures with 5 wt% loss.

biphenyl moieties in its optimized structures derived from calculation show twisted geometry with dihedral angles of *ca.* 36.5°.

The electronic densities of HOMOs and LUMOs for the two objective complexes are depicted in Fig. 5, and the calculated HOMO and LUMO energy level data are summarized in Table 2. Although the calculated LUMOs are significantly higher, and the HOMOs are slightly higher than the experimental data, the variation trends for both frontier orbital energies and energy gaps of the complexes show perfect reproduction between the computation and experiment values. In accordance with the electrochemical measurements, the (methoxy)phenyl substituents are found to contribute to the HOMOs rather than LUMOs of the complexes. Generally, the HOMO energy level of **(bt)$_2$Ir(acac)** is dominated by Ir-d orbitals and π-orbitals of phenyl moieties,[39] thus the elevated HOMO of the target compounds should be attributed to the effectively elongated conjugation system arising from the (methoxy)phenyl substituents in the *para*-site of C–Ir bonds. On the contrary, as the LUMO of **(bt)$_2$Ir(acac)** predominantly localizes on the π* orbitals of benzothiazole segments,[39] the phenyl substituent should contribute little to the LUMO due to the poor electron-coupling at the *meta*-site of **bt** ligand. Meanwhile in the case of **(4Phbt)$_2$Ir(acac)**, the *para*-phenyl substituent is found to contribute to LUMO rather than HOMO.[22a]

Electroluminescence properties

Based on the CV and photophysical experimental results, PVK is selected as host material for these iridium complexes to realize exothermic energy transfer, and solution-processed single-layered PhOLEDs using these chelates as dopants have been fabricated. The configuration of the devices is: ITO/PEDOT:PSS (40 nm)/PVK:OXD-7:Ir complex (67 : 27 : 6 in wt%) (70 nm)/Ba (3 nm)/Al (120 nm), where ITO acts as anode, PEDOT:PSS as hole-injecting layer, PVK as hole-transporting host, OXD-7 as electron-transporting material, and Ba/Al as the cathode. A doping level of 6 wt% for the guest compound is used according to the PLQY measurements, so that a compromise between adequate luminescence site for carrier recombination and minor concentration quenching could be reached. The reference device I using **(bt)$_2$Ir(acac)** as guest has been fabricated for comparison, and devices II, III and IV represent PhOLEDs with **(4Phbt)$_2$Ir(acac)**, **(3Phbt)$_2$Ir(acac)** and **(3OMePhbt)$_2$Ir(acac)** as phosphorescent guests, respectively. The relative energy level alignment of the devices and the molecular structures of the chemicals used are shown in Fig. 6.

The EL spectra of the devices are shown in Fig. 7. Devices I and II exhibit orange and orange-red emission with λ_{ELmax} of 564 nm and 584 nm, and CIE coordinates of (0.51, 0.49) and (0.57, 0.42), respectively, while the devices III and IV emit orange light with λ_{ELmax} of 570 and 578 nm, and CIE coordinates of (0.52, 0.47) and (0.55, 0.45), respectively. In each case, the EL spectrum basically resembles the corresponding PL spectrum of the blend film except for the relative intensity of the shoulder peak (Fig. S10†), implying that the EL emission originates from radiative decay of the phosphors. Consistent with the PL measurements, the λ_{ELmax} of devices II, III and IV are red-shifted compared to device I. As compared with PVK and OXD-7, all the dopants possess higher lying HOMOs and lower lying LUMOs, taking into account that the doping concentration is 6 wt%, the holes and electrons should be mainly injected into PVK and OXD-7, respectively, yet some of the charge carriers should also be injected directly into the phosphors, *i.e.*, the phosphors may act as the carrier trapping sites to form excitons. The absence of emission from either PVK or

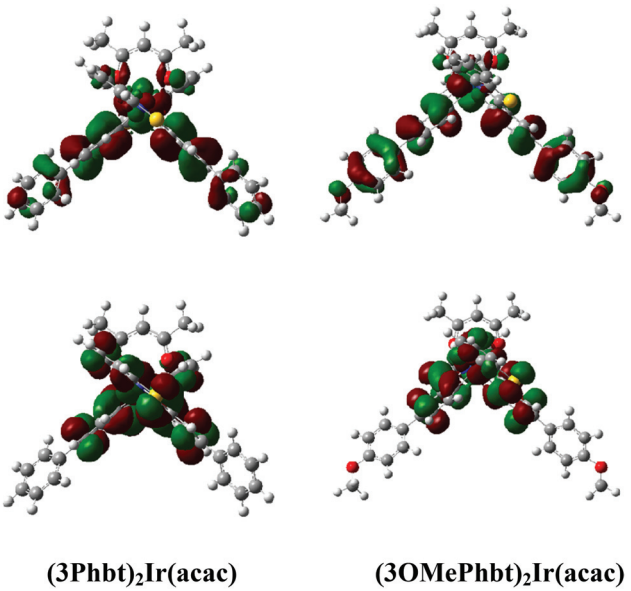

Fig. 5 Isodensity plots of the HOMOs (top) and LUMOs (bottom) for **(3Phbt)$_2$Ir(acac)** and **(3OMePhbt)$_2$Ir(acac)**.

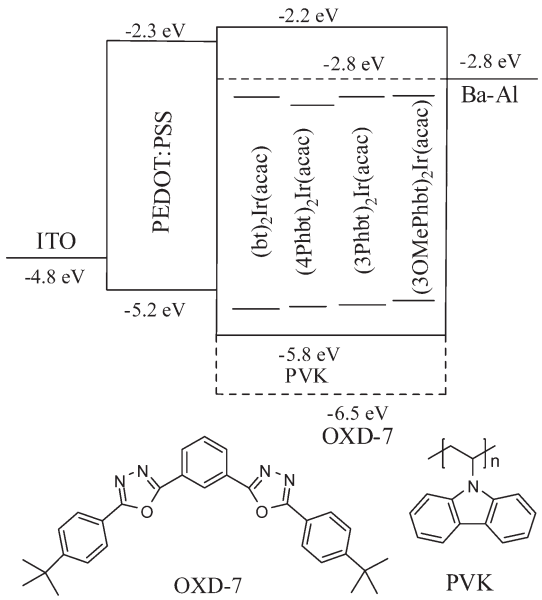

Fig. 6 Device configuration and energy band diagram of the PhOLEDs, and the molecular structures of the compounds used.

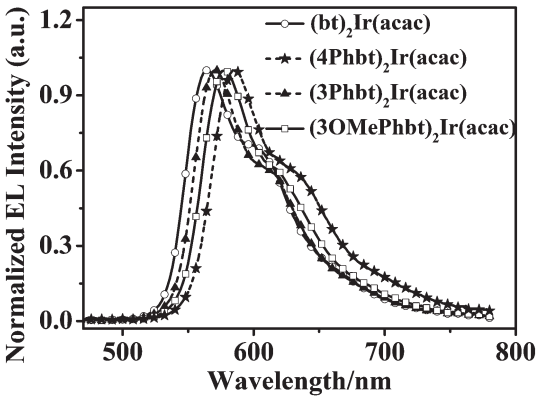

Fig. 7 EL spectra of the PhOLEDs at current density of 13.3 mA cm^{-2}.

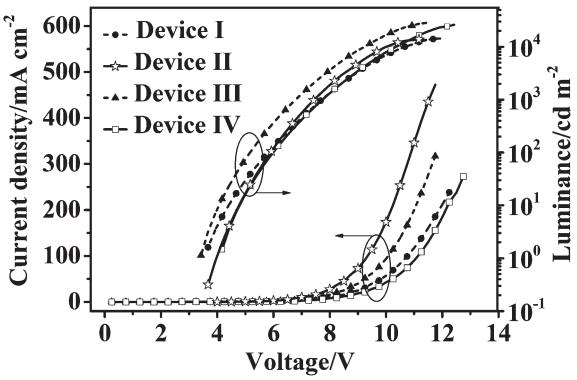

Fig. 8 Current density–voltage–luminance characteristics of the devices.

OXD-7 in these devices suggests effective energy transfer and/or charge carrier trapping on the guests during the EL emission procedure.

The corresponding current density–voltage–luminance (*J–V–L*) characteristics of the devices are shown in Fig. 8, and some representative data are summarized in Table 3. The turn-on voltage of devices I, II, III and IV is 4.0, 4.2, 3.7 and 4.4 V in sequence. Compared with device I, devices II and III show higher current density at identical driven voltage, which might be attributed to the more efficient carrier trapping arising from the relatively lower lying LUMO energy level of **$(4Phbt)_2$-Ir(acac)**, and higher lying HOMO energy level of **$(3Phbt)_2$-Ir(acac)**, whereas the slightly lower current density of **$(3OMePhbt)_2Ir(acac)$**-based device IV might be ascribed to the presence of electrically insulating methoxy substituents that may induce reduced carrier mobility.[22b,35,40] Nevertheless, although the current density of device II is much higher than all the other three devices at voltages of >7 V, its luminance is just comparable to device I and IV in 7–11 V, but inferior to that of device III, *i.e.*, device II exhibits much lower current efficiency relative to the other devices, indicative of the more severe self-quenching of the **$(4Phbt)_2Ir(acac)$** phosphor, and/or worse carrier balance in device II. Devices III and IV exhibit orange emission with maximum brightness of 28 270 and 27 900 cd m^{-2}, respectively, almost twice as bright as that of device I (14 350 cd m^{-2}) and device II (13 970 cd m^{-2}). As shown in Fig. 9, devices III and IV display maximum current efficiencies (η_{Lmax}) of 17.2 and 15.2 cd A^{-1} respectively, both are drastically enhanced compared to the devices I and II (10.2 and 5.0 cd A^{-1}, respectively). It is noteworthy that η_{Lmax} values of devices III and IV are obtained under luminance of >2500 cd m^{-2}, and furthermore, satisfied efficiency could be achieved even at higher brightness (Fig. 9). For example, η_L of device III remains as high as 16.3 cd A^{-1} at 5000 cd m^{-2} with roll-off of only 5.2%, and 15.4 cd A^{-1} at 10 000 cd m^{-2} with roll-off of only 10.5%; moreover, high η_L of 12.8 and 10.7 cd A^{-1} could even be achieved at 20 000 and 25 000 cd m^{-2}, respectively. In the case of device IV, η_L is found to be as high as 15.1 cd A^{-1} at 5000 cd m^{-2} with negligible efficiency roll-off, and 14.2 cd A^{-1} at 10 000 cd m^{-2} with 6.6% roll-off; while high η_Ls of 11.9 and 10.0 cd A^{-1} could be achieved at 20 000 and 25 000 cd m^{-2}. In comparison, device I shows analogous low η_L roll-off at J < 200 mA cm^{-2} with devices III and IV, yet more severe roll-off is observed at higher driving current density. For instance, at current density of 250 and 300 mA cm^{-2}, device I exhibits η_L roll-off of 43.1% and 57.8%, whereas that of device III is 39.5% and 45.9%, and that of device IV is 35.5% and 40.8%, respectively. However, device II with **$(4Phbt)_2Ir(acac)$** as phosphor shows a more suppressed η_L roll-off than the other three devices, which exhibits η_L roll-off of 14.0% and 20.0% at current density of 250 and 300 mA cm^{-2}, respectively. The lower efficiencies roll-off of device II might be attributed to the much better thermal stability of **$(4Phbt)_2Ir(acac)$**. It should be pointed out that in despite of their inferior η_{Lmax} relative to those high performance single-layered PhOLEDs,[6a,d,e,19c] devices III and IV display rather low efficiency roll-off, and high η_L of ~12 cd A^{-1} could be even achieved at 20 000 cd m^{-2}, which is comparable to the best PhOLEDs reported so far.[5d,f,6a,6d–f,19c]

Table 3 EL characteristics of the devices

Device	$V_{turn\text{-}on}$ (V)	L_{max}[a] (cd m^{-2}) (V)	η_{pmax}[b] (lm W^{-1})	η_L[c] (cd A^{-1})	η_L[d] (cd A^{-1})	CIE (x, y)
I	4.0	14 350 (12.3)	3.8 (960, 8.0)	10.2, 10.0, 8.6, —, —	10.0, 8.9, 7.8, 6.9, 5.8, 4.3	(0.51, 0.49)
II	4.2	13 790 (11.5)	1.9 (1310, 8.0)	5.0, 4.9, 4.4, —, —	4.9, 4.8, 4.7, 4.5, 4.2, 4.0	(0.57, 0.42)
III	3.7	28 270 (11.8)	7.6 (640, 6.8)	17.2, 16.3, 15.4, 12.8, 10.7	15.8, 14.1, 12.9, 11.7, 10.4, 9.3	(0.52, 0.47)
IV	4.4	27 900 (13.3)	5.3 (2030, 8.8)	15.2, 15.1, 14.2, 11.9, 10.0	14.8, 13.1, 12.2, 11.2, 9.8, 9.0	(0.55, 0.45)

[a] Data in parentheses are the corresponding driven voltages (V). [b] Data in parentheses are the corresponding EL brightness (cd m^{-2}) and driven voltages (V). [c] Order of measured value: maximum, then values at 5000, 10 000, 20 000 and 25 000 cd m^{-2} in sequence. [d] Order of measured value: values at 50, 100, 150, 200, 250 and 300 mA cm^{-2} in sequence.

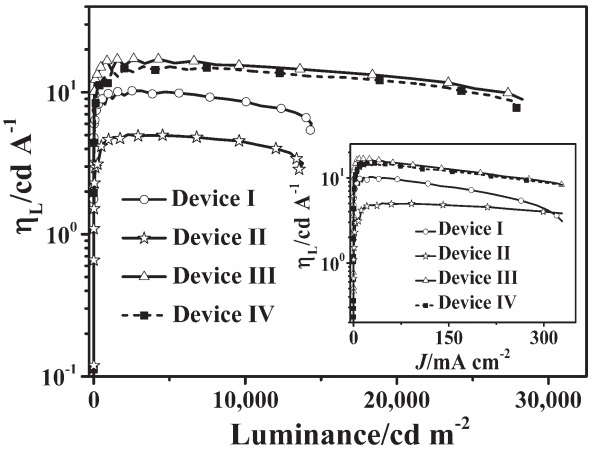

Fig. 9 Current efficiency–luminance and current efficiency–current density characteristics (inset) of the devices.

Although the PLQYs of as-prepared **(4Phbt)$_2$Ir(acac)**-blended films are the lowest among all these four compounds, the 6 wt% doped film just displays slightly decreased PLQY (20% decrease) after thermo-annealing (140 °C, 30 min), indicative of its better thermal stability. In contrast, although the as-prepared 6 wt% **(bt)$_2$Ir(acac)** blended film (in PVK) shows higher PL efficiency, the PLQY of the sample is found to drop dramatically upon annealing. Note that thermal treatment is a general fabrication procedure for OLEDs to ensure complete removal of solvents, and to improve the efficiency and reduce the driving voltage as well.[41] As depicted in Table 1, after thermal annealing, **(bt)$_2$Ir(acac)**-doped film exhibits steeply 45% decreased PLQY, while **(3Phbt)$_2$Ir(acac)** and **(3OMePhbt)$_2$Ir(acac)**-doped films show 16% and 18% decrease on PLQY, respectively. It is suspected that the thermal treatment would influence the morphological and photophysical characteristics of the thin films. Using AFM in tapping mode, the morphological stability of these pre- and post-annealed 6 wt% doped films have been investigated (Fig. 10, with phase images acquired concurrently with the height mode). Clearly evidenced by these images, the as-prepared films show smooth and homogenous surfaces with the root-mean-square (RMS) of 0.23–0.31 nm, suggesting that these complexes could be dispersed evenly in PVK. After annealing, the surface roughness of **(bt)$_2$Ir(acac)**-doped film increases significantly with RMS varied from 0.27 to 0.60 nm, and the newly emerged small crystalline domains are found to have an average height reaching 4.6 nm (Fig. 10b), indicative of the aggregation of **(bt)$_2$Ir(acac)** molecules upon annealing. In the case of **(4Phbt)$_2$Ir(acac)**-based film, small crystalline domains could even be found in the as-prepared films, and the average height is 4.7 nm, while after thermal-annealing, the average height increases to 8.1–9.3 nm, and the RMS of the blended films varies just slightly from 0.31 nm to 0.40 nm. In contrast, the as-prepared **(3Phbt)$_2$Ir(acac)**- and **(3OMePhbt)$_2$Ir(acac)**-blended films are smooth and homogenous, while upon thermal treatment, their RMS increase only slightly (RMS varied from 0.25 nm to 0.34 nm, and 0.23 nm to 0.29 nm, respectively). Therefore, **(3Phbt)$_2$Ir(acac)** and **(3OMePhbt)$_2$Ir(acac)** bearing *meta*-phenyl substitutes are confirmed to show enhanced film morphological stability relative to **(bt)$_2$Ir(acac)** and **(4Phbt)$_2$Ir(acac)**, which is beneficial for the alleviation of self-quenching and TTA under higher working temperatures or upon thermal treatment. Taking into account that the PLQYs of the active layers in devices I and II are much lower than those of devices III and IV, the relatively higher luminance, efficiency and reduced efficiency roll-off at high current density for the PhOLEDs III and IV should mainly be

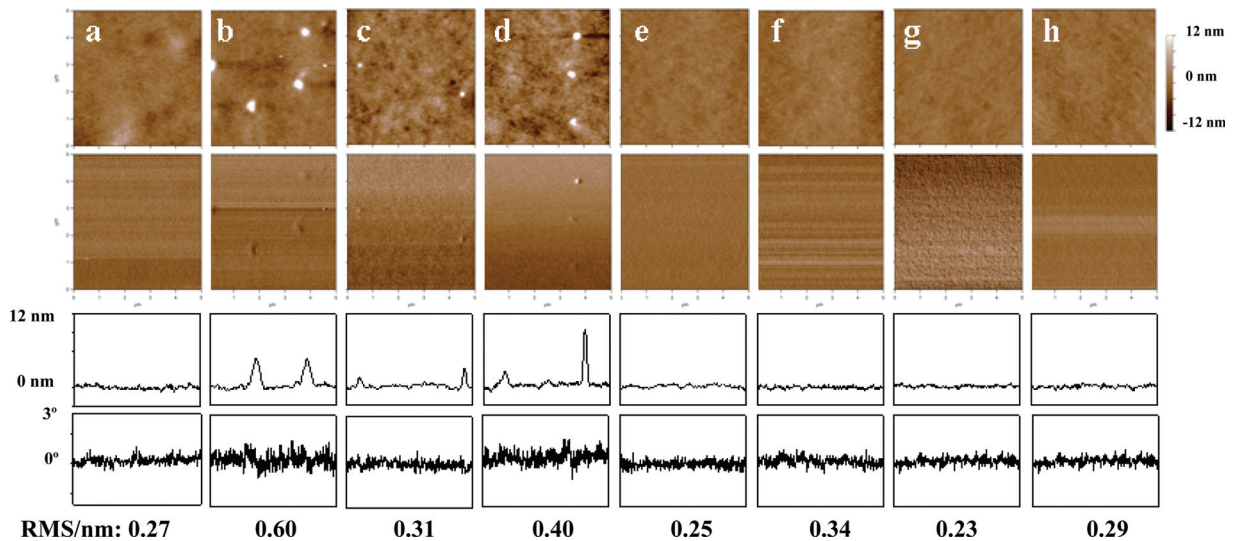

Fig. 10 Typical AFM images of height mode (upper row), phase mode (second row), cross section view of height modes (third row), and phase modes (bottom row) for Ir complexes/PVK blended films (6 wt%) before and after thermo-annealing (140 °C for 30 min in vacuum). **(bt)$_2$Ir(acac)**-doped samples: (a) as-prepared, (b) post-annealed; **(4Phbt)$_2$Ir(acac)**-doped samples: (c) as-prepared, (d) post-annealed; **(3Phbt)$_2$Ir(acac)**-doped samples: (e) as-prepared, (f) post-annealed; **(3OMePhbt)$_2$Ir(acac)**-doped samples: (g) as-prepared, (h) post-annealed. All scan scales for the images are 5.00 × 5.00 μm.

attributed to the enhanced film morphological stability and amorphism of the active layers, in addition to the aforementioned improved carrier balance.

It should be pointed out that compared with state-of-art phosphorescent Ir complexes, PLQYs of the active layers based on these complexes are not high, which may eventually limit device efficiency. Nevertheless, we believe that their PLQYs can be improved by utilizing other host materials instead of PVK, or introducing a blue or green light emitting sensitizer. Moreover, the device structure, doping level, and layer thickness used here have not been optimized for either low driven voltage or high efficiency, thus much improved EL performance should be expected after further optimization has been carried out on these issues.

Conclusions

By phenyl-modification of the phenyl moiety of **bt** ligand, the resulting complexes are found to exhibit enhanced thermal and morphological stability relative to their parent complex **(bt)$_2$Ir(acac)**. Nevertheless, the compound bearing *para*-phenyl shows a strong tendency to crystallize due to the presence of intense intermolecular interaction; whereas those with *meta*-substituted one, *i.e.* **(3Phbt)$_2$Ir(acac)** and **(3OMePhbt)$_2$Ir(acac)**, possess drastically enhanced processability with good film amorphism. Consequently, **(3Phbt)$_2$Ir(acac)** and **(3OMePhbt)$_2$Ir(acac)** show much improved EL performances relative to **(bt)$_2$Ir(acac)** and **(4Phbt)$_2$Ir(acac)**. Single-layered solution-processed PhOLEDs based on them display L_{max} of 28 270 cd m^{-2} and η_{Lmax} of 17.2 cd A^{-1}, with quite low efficiency roll-off at high luminance of even 20 000 cd m^{-2}. All these preliminary results reveal that the phenylation on ligands at appropriate site is a simple yet effective means for the enhancement of film amorphism, and the two resulting complexes are very promising phosphorescent guests for application in large-area PhOLEDs with low costs.

Acknowledgements

The authors acknowledge the financial support for this work by the National Natural Science Foundation of China (Projects 21072139, 21190031, 51073057, 91233116 and U1230121), and the Open Fund of the State Key Laboratory of Luminescent Materials and Devices (South China University of Technology). We are grateful to the analytical and testing center of Sichuan University for providing NMR and X-ray single crystal analyses of the intermediates and objective compounds.

References

1 (*a*) M. A. Baldo, Y. You, A. Shoustikov, S. Sibley, M. E. Thompson and S. R. Forrest, *Nature*, 1998, **395**, 151; (*b*) M. A. Baldo, S. Lamansky, P. E. Burrows, M. E. Thompson and S. R. Forrest, *Appl. Phys. Lett.*, 1999, **75**, 4.

2 (*a*) D. Tanaka, H. Sasabe, Y.-J. Li, S.-J. Su, T. Takeda and J. Kido, *Jpn. J. Appl. Phys.*, 2007, **46**, L10; (*b*) C.-H. Fan, P. Sun, T.-H. Su and C.-H. Cheng, *Adv. Mater.*, 2011, **23**, 2981; (*c*) R. Wang, D. Liu, H. Ren, T. Zhang, H. Yin, G. Liu and J. Li, *Adv. Mater.*, 2011, **23**, 2823; (*d*) D. H. Kim, N. S. Cho, H.-Y. Oh, J. H. Yang, W. S. Jeon, J. S. Park, M. C. Suh and J. H. Kwon, *Adv. Mater.*, 2011, **23**, 2721; (*e*) T. Peng, Y. Yang, H. Bi, Y. Liu, Z. Hou and Y. Wang, *J. Mater. Chem.*, 2011, **21**, 3551; (*f*) R. Wang, D. Liu, H. Ren, T. Zhang, X. Wang and J. Li, *J. Mater. Chem.*, 2011, **21**, 15494; (*g*) S.-J. Su, C. Cai and J. Kido, *J. Mater. Chem.*, 2012, **22**, 3447; (*h*) R. Wang, L. Deng, T. Zhang and J. Li, *Dalton Trans.*, 2012, **41**, 6833; (*i*) G. Tan, S. Chen, N. Sun, Y. Li, D. Fortin, W.-Y. Wong, H.-S. Kwok, D. Ma, H. Wu, L. Wang and P. D. Harvey, *J. Mater. Chem. C*, 2013, **1**, 808.

3 (*a*) C. A. Zuniga, S. Barlow and S. R. Marder, *Chem. Mater.*, 2011, **23**, 658; (*b*) E. Ahmed, T. Earmme and S. A. Jenekhe, *Adv. Funct. Mater.*, 2011, **21**, 3889; (*c*) J. Chen, C. Shi, Q. Fu, F. Zhao, Y. Hu, Y. Feng and D. Ma, *J. Mater. Chem.*, 2012, **22**, 5164; (*d*) S. Hu, M. Zhu, Q. Zou, H. Wu and C. Yang, *Appl. Phys. Lett.*, 2012, **100**, 063304.

4 (*a*) H. Wu, L. Ying, W. Yang and Y. Cao, *Chem. Soc. Rev.*, 2009, **38**, 3391; (*b*) M. Cai, T. Xiao, E. Hellerich, Y. Chen, R. Shinar and J. Shinar, *Adv. Mater.*, 2011, **23**, 3590; (*c*) S. Gong, C. Yang and J. Qin, *Chem. Soc. Rev.*, 2012, **41**, 4797.

5 (*a*) K. S. Yook and J. Y. Lee, *Org. Electron.*, 2011, **12**, 1711; (*b*) S.-J. Kim, Y. Zhang, C. Zuniga, S. Barlow, S. R. Marder and B. Kippelen, *Org. Electron.*, 2011, **12**, 492; (*c*) Q. Mei, L. Wang, Y. Guo, J. Weng, F. Yan, B. Tian and B. Tong, *J. Mater. Chem.*, 2012, **22**, 6878; (*d*) B. Zhang, G. Tan, C.-S. Lam, B. Yao, C.-L. Ho, L. Liu, Z. Xie, W.-Y. Wong, J. Ding and L. Wang, *Adv. Mater.*, 2012, **24**, 1873; (*e*) J. Li, T. Zhang, Y. Liang and R. Yang, *Adv. Funct. Mater.*, 2013, **23**, 46; (*f*) J.-H. Jou, C.-H. Chen, J.-R. Tseng, S.-H. Peng, P.-W. Chen, C.-I. Chiang, Y.-C. Jou, C.-C. Wang, C.-C. Chen, F.-C. Tung, S.-H. Chen, Y.-S. Wang and C.-L. Chinc, *J. Mater. Chem. C*, 2013, **1**, 394.

6 (*a*) H. Wu, G. Zhou, J. Zou, C.-L. Ho, W.-Y. Wong, W. Yang, J. Peng and Y. Cao, *Adv. Mater.*, 2009, **21**, 4181; (*b*) H. A. Al-Attar, G. C. Griffiths, T. N. Moore, M. Tavasli, M. A. Fox, M. R. Bryce and A. P. Monkman, *Adv. Funct. Mater.*, 2011, **21**, 2376; (*c*) M. Zhu, Y. Li, S. Hu, C. Li, C. Yang, H. Wu, J. Qin and Y. Cao, *Chem. Commun.*, 2012, **48**, 2695; (*d*) M. Zhu, J. Zou, S. Hu, C. Li, C. Yang, H. Wu, J. Qin and Y. Cao, *J. Mater. Chem.*, 2012, **22**, 361; (*e*) X. Ouyang, D. Chen, S. Zeng, X. Zhang, S.-J. Su and Z. Ge, *J. Mater. Chem.*, 2012, **22**, 23005; (*f*) M. Zhu, J. Zou, X. He, C. Yang, H. Wu, C. Zhong, J. Qin and Y. Cao, *Chem. Mater.*, 2012, **24**, 174.

7 (*a*) Y. H. Song, S. J. Yeh, C. T. Chen, Y. Chi, C. S. Liu, J. K. Yu, Y. H. Hu, P. T. Chou, S. M. Peng and G. H. Lee, *Adv. Funct. Mater.*, 2004, **14**, 1221; (*b*) K. Zhang, Z. Chen, C. Yang, X. Zhang, Y. Tao, L. Duan, L. Chen, L. Zhu, J. Qin

and Y. Cao, *J. Mater. Chem.*, 2007, **17**, 3451; (*c*) J.-Y. Yu, I.-W. P. Chen, C.-H. Chen, S.-J. Lee, I.-C. Chen, C.-S. Lin and C.-H. Cheng, *J. Phys. Chem. C*, 2008, **112**, 3097.

8 R. Wang, D. Liu, R. Zhang, L. Deng and J. Li, *J. Mater. Chem.*, 2012, **22**, 1411.

9 X. Yang, D. Neher, D. Hertel and T. K. Daubler, *Adv. Mater.*, 2004, **16**, 161.

10 (*a*) T. Qin, J. Ding, L. Wang, M. Baumgarten, G. Zhou and K. Mullen, *J. Am. Chem. Soc.*, 2009, **131**, 14329; (*b*) L. Chen, Z. Ma, J. Ding, L. Wang, X. Jing and F. Wang, *Chem. Commun.*, 2011, **47**, 9519; (*c*) S. Gambino, S.-C. Lo, Z. Liu, P. L. Burn and I. D. W. Samuel, *Adv. Funct. Mater.*, 2012, **22**, 157; (*d*) T. Qin, J. Ding, M. Baumgarten, L. Wang and K. Müllen, *Macromol. Rapid Commun.*, 2012, **33**, 1036; (*e*) L. Chen, Z. Ma, J. Ding, L. Wang, X. Jing and F. Wang, *Org. Electron.*, 2012, **13**, 2160.

11 (*a*) J. H. Yao, C. Zhen, K. P. Loh and Z.-K. Chen, *Tetrahedron*, 2008, **64**, 10814; (*b*) L.-H. Xie, R. Zhu, Y. Qian, R.-R. Liu, S.-F. Chen, J. Lin and W. Huang, *J. Phys. Chem. Lett.*, 2010, **1**, 272; (*c*) S.-O. Kim, Q. Zhao, K. Thangaraju, J. J. Kim, Y.-H. Kim and S.-K. Kwon, *Dyes Pigm.*, 2011, **90**, 139; (*d*) S. Shao, Z. Ma, J. Ding, L. Wang, X. Jing and F. Wang, *Adv. Mater.*, 2012, **24**, 2009.

12 C. Ulbricht, B. Beyer, C. Friebe, A. Winter and U. S. Schubert, *Adv. Mater.*, 2009, **21**, 4418.

13 (*a*) G.-J. Zhou, W.-Y. Wong, B. Yao, Z. Xie and L. Wang, *J. Mater. Chem.*, 2008, **18**, 1799; (*b*) T. Peng, H. Bi, Y. Liu, Y. Fan, H. Gao, Y. Wang and Z. Hou, *J. Mater. Chem.*, 2009, **19**, 8072; (*c*) Y. You and S. Y. Park, *Dalton Trans.*, 2009, 1267; (*d*) K. H. Lee, H. J. Kang, J. K. Park, J. H. Seo, Y. K. Kim and S. S. Yoon, *Thin Solid Films*, 2010, **518**, 6188; (*e*) F. Kessler, Y. Watanabe, H. Sasabe, H. Katagiri, M. K. Nazeeruddin, M. Grätzel and J. Kido, *J. Mater. Chem. C*, 2013, **1**, 1070.

14 (*a*) M. Velusamy, K. R. J. Thomas, C.-H. Chen, J. T. Lin, Y. S. Wen, W.-T. Hsieh, C.-H. Lai and P.-T. Chou, *Dalton Trans.*, 2007, 3025; (*b*) J.-Y. Yu, M.-J. Huang, C.-H. Chen, C.-S. Lin and C.-H. Cheng, *J. Phys. Chem. C*, 2009, **113**, 7405; (*c*) J. Xiao, S. Liu, Y. Liu, L. Ji, X. Liu, H. Zhang, X. Sun and Q. Zhang, *Chem.–Asian J.*, 2012, **7**, 561; (*d*) L. Deng, X. Wang, Z. Zhang and J. Li, *J. Mater. Chem.*, 2012, **22**, 19700.

15 (*a*) J. N. Moorthy, P. Venkatakrishnan, P. Natarajan, D.-F. Huang and T. J. Chow, *J. Am. Chem. Soc.*, 2008, **130**, 17320; (*b*) Y. Zou, T. Ye, D. Ma, J. Qina and C. Yang, *J. Mater. Chem.*, 2012, **22**, 23485.

16 (*a*) Z. Jiang, T. Ye, C. Yang, D. Yang, M. Zhu, C. Zhong, J. Qin and D. Ma, *Chem. Mater.*, 2011, **23**, 771; (*b*) H. Huang, Y. Wang, S. Zhuang, X. Yang, L. Wang and C. Yang, *J. Phys. Chem. C*, 2012, **116**, 19458.

17 (*a*) Z. Liu, M. Guan, Z. Bian, D. Nie, Z. Gong, Z. Li and C. Huang, *Adv. Funct. Mater.*, 2006, **16**, 1441; (*b*) Y. J. Cho and J. Y. Lee, *Adv. Mater.*, 2011, **23**, 4568.

18 (*a*) J. N. Moorthy, P. Venkatakrishnan, P. Natarajan, Z. Lin and T. J. Chow, *J. Org. Chem.*, 2010, **75**, 2599; (*b*) S.-H. Lin, F.-I. Wu, H.-Y. Tsai, P.-Y. Chou, H.-H. Chou, C.-H. Cheng and R.-S. Liu, *J. Mater. Chem.*, 2011, **21**, 8122; (*c*) M.-G. Shin, S. O. Kim, H. T. Park, S. J. Park, H. S. Yu, Y.-H. Kim and S.-K. Kwon, *Dyes Pigm.*, 2012, **92**, 1075.

19 (*a*) J. C. Ostrowski, M. R. Robinson, A. J. Heeger and G. C. Bazan, *Chem. Commun.*, 2002, 784; (*b*) S. Bettington, M. Tavasli, M. R. Bryce, A. Beeby, H. Al-Attar and A. P. Monkman, *Chem.–Eur. J.*, 2007, **13**, 1423; (*c*) A. M'hamedi, A. S. Batsanov, M. A. Fox, M. R. Bryce, K. Abdullah, H. A. Al-Attar and A. P. Monkman, *J. Mater. Chem.*, 2012, **22**, 13529.

20 (*a*) C.-L. Ho, W.-Y. Wong, G.-J. Zhou, B. Yao, Z. Xie and L. Wang, *Adv. Funct. Mater.*, 2007, **17**, 2925; (*b*) C.-L. Ho, Q. Wang, C.-S. Lam, W.-Y. Wong, D. Ma, L. Wang, Z.-Q. Gao, C.-H. Chen, K.-W. Cheah and Z. Lin, *Chem.–Asian J.*, 2009, **4**, 89; (*c*) M. Tavasli, T. N. Moore, Y. Zheng, M. R. Bryce, M. A. Fox, G. C. Griffiths, V. Jankus, H. A. Al-Attar and A. P. Monkman, *J. Mater. Chem.*, 2012, **22**, 6419; (*d*) F.-F. Yu, H.-L. Fan, H.-F. Huang, Q.-Y. Cao, Y.-F. Dai, X.-C. Gao, Y.-Z. Shang, M.-Y. Zhang, L. Long, H. Xu, X.-F. Li and B. Wei, *Inorg. Chim. Acta*, 2012, **390**, 119.

21 (*a*) T. Tsuzuki, N. Shirasawa, T. Suzuki and S. Tokito, *Adv. Mater.*, 2003, **15**, 1455; (*b*) N. Rehmann, D. Hertel, K. Meerholz, H. Becker and S. Heun, *Appl. Phys. Lett.*, 2007, **91**, 103507; (*c*) L. Sun, A. Galan, S. Ladouceur, J. D. Slinker and E. Zysman-Colman, *J. Mater. Chem.*, 2011, **21**, 18083.

22 (*a*) M. Li, H. Zeng, Y. Meng, H. Sun, S. Liu, Z. Lu, Y. Huang and X. Pu, *Dalton Trans.*, 2011, **40**, 7153; (*b*) M. Li, Q. Wang, J. Dai, Z.-Y. Lu, Y. Huang, J.-S. Yu, S. Luo and S.-J. Su, *Thin Solid Films*, 2012, **526**, 231; (*c*) Q. Wang, J.-S. Yu, J. Zhao, M. Li and Z.-Y. Lu, *J. Phys. D: Appl. Phys.*, 2013, **46**, 155102; (*d*) Q. Wang, J.-S. Yu, J. Zhao, J. Wang, M. Li and Z.-Y. Lu, *J. Lumin.*, 2013, **134**, 870.

23 Oxford Diffraction, *CrysAlisPro CCD and CrysAlisPro RED, including ABSPACK*, Oxford Diffraction Ltd, Yarnton, England, 2009.

24 A. L. Spek, *J. Appl. Crystallogr.*, 2003, **36**, 7.

25 (*a*) A. D. Becke, *J. Chem. Phys.*, 1993, **98**, 5648; (*b*) C. Lee, W. Yang and R. G. Parr, *Phys. Rev. B.: Condens. Matter*, 1988, **37**, 785.

26 P. J. Hay, *J. Phys. Chem. A*, 2002, **106**, 1634.

27 E. Cancès, B. Mennucci and J. Tomasi, *J. Chem. Phys.*, 1997, **107**, 3032.

28 M. J. Frisch, G. W. Trucks, H. B. Schlegel, G. E. Scuseria, M. A. Robb, J. R. Cheeseman, G. Scalmani, V. Barone, B. Mennucci, G. A. Petersson, H. Nakatsuji, M. Caricato, X. Li, H. P. Hratchian, A. F. Izmaylov, J. Bloino, G. Zheng, J. L. Sonnenberg, M. Hada, M. Ehara, K. Toyota, R. Fukuda, J. Hasegawa, M. Ishida, T. Nakajima, Y. Honda, O. Kitao, H. Nakai, T. Vreven, J. A. Montgomery, Jr., J. E. Peralta, F. Ogliaro, M. Bearpark, J. J. Heyd, E. Brothers, K. N. Kudin, V. N. Staroverov, R. Kobayashi, J. Normand, K. Raghavachari, A. Rendell, J. C. Burant, S. S. Iyengar, J. Tomasi, M. Cossi, N. Rega, J. M. Millam, M. Klene, J. E. Knox, J. B. Cross, V. Bakken, C. Adamo, J. Jaramillo, R. Gomperts, R. E. Stratmann, O. Yazyev, A. J. Austin, R. Cammi, C. Pomelli, J. Ochterski, R. L. Martin, K. Morokuma, V. G. Zakrzewski,

G. A. Voth, P. Salvador, J. J. Dannenberg, S. Dapprich, A. D. Daniels, O. Farkas, J. B. Foresman, J. V. Ortiz, J. Cioslowski and D. J. Fox, *GAUSSIAN 09 (Revision A.2)*, Gaussian, Inc., Wallingford, CT, 2009.

29 J. M. Cary and J. S. Moore, *Org. Lett.*, 2002, **4**, 4663.

30 W. Y. Huang and S. Y. Huang, *Macromolecules*, 2010, **43**, 10355.

31 J. Charton, S. Girault-Mizzi, M.-A. Debreu-Fontaine, F. Foufelle, I. Hainault, D.-H. Caignard and C. Sergheraert, *Bioorg. Med. Chem.*, 2006, **14**, 4490.

32 I. R. Laskar and T. M. Chen, *Chem. Mater.*, 2004, **16**, 111.

33 (*a*) F. O. Garces, K. A. King and R. J. Watts, *Inorg. Chem.*, 1988, **27**, 3464; (*b*) S. Sprouse, K. A. King, P. J. Spellane and R. J. Watts, *J. Am. Chem. Soc.*, 1984, **106**, 6647.

34 W. Jiang, L. Duan, J. Qiao, D. Zhang, G. Dong, L. Wang and Y. Qiu, *J. Mater. Chem.*, 2010, **20**, 6131.

35 S. Ye, Y. Liu, K. Lu, W. Wu, C. Du, Y. Liu, H. Liu, T. Wu and G. Yu, *Adv. Funct. Mater.*, 2010, **20**, 3125.

36 (*a*) A. Tsuboyama, H. Iwawaki, M. Furugori, T. Mukaide, J. Kamatani, S. Igawa, T. Moriyama, S. Miura, T. Takiguchi, S. Okada, M. Hoshino and K. Ueno, *J. Am. Chem. Soc.*, 2003, **125**, 12971; (*b*) J. P. Duan, P. P. Sun and C. H. Cheng, *Adv. Mater.*, 2003, **15**, 224.

37 H. A. Bronstein, C. E. Finlayson, K. R. Kirov, R. H. Friend and C. K. Williams, *Organometallics*, 2008, **27**, 2980.

38 K. R. J. Thomas, M. Velusamy, J. T. Lin, C. H. Chien, Y. T. Tao, Y. S. Wen, Y. H. Hu and P. T. Chou, *Inorg. Chem.*, 2005, **44**, 5677.

39 A. B. Tamayo, B. D. Alleyne, P. I. Djurovich, S. Lamansky, I. Tsyba, N. N. Ho, R. Bau and M. E. Thompson, *J. Am. Chem. Soc.*, 2003, **125**, 7377.

40 M. Zhu, Q. Wang, Y. Gu, X. Cao, C. Zhong, D. Ma, J. Qin and C. Yang, *J. Mater. Chem.*, 2011, **21**, 6409.

41 (*a*) T.-W. Lee and O. O. Park, *Appl. Phys. Lett.*, 2000, **77**, 3334; (*b*) J. Liu, T.-F. Guo and Y. Yang, *J. Appl. Phys.*, 2002, **91**, 1595.